The published version is available at: http://dx.doi.org/10.1109/SPEEDAM.2010.5544811

Modeling the Effect of Inverter Supply on Eddy-Current Losses in Synchronous Machines

Paavo Rasilo and Antero Arkkio
Department of Electrical Engineering, Aalto University School of Science and Technology
P.O. Box 13000 FI-00076 Aalto, Finland
paavo.rasilo@tkk.fi

***Abstract*—The effect of inverter supply on the eddy-current losses in the laminated core of a synchronous machine is studied. A 2D finite element model including a dynamic model for the eddy currents in the core laminations is applied to predict the machine losses by numerical simulations. A synchronous extruder motor is simulated both with sinusoidal and pulse-width modulated voltage supplies in different operating points and the eddy-current losses both in the stator and the rotor are studied. The rotor additional inverter losses are found to be load-dependent while the stator additional losses remain constant independent of the loading.**

***Index Terms*—Eddy currents, finite element methods, pulse width modulated inverters, synchronous machines.**

I. Introduction

An increasing number of electrical motors is supplied from frequency converters. Controlling the rotation speed by varying the supply frequency is essential in process industry and propulsion applications and can in addition allow huge energy savings when applied e.g. to pumps, compressors or extrusion processes. However, the non-sinusoidal supply voltage from the frequency converter causes additional energy losses in the motors. Since the output voltages are formed by controlled switching using thyristors or power transistors, the frequency contents can consist of harmonic components up to tens of kilohertz. Thus the current drawn by the inverter-supplied motor also contains high-frequency harmonics which increase the machine losses due to skin effect in the armature windings, additional hysteresis losses caused by the distorted flux-density waveforms and increased eddy-currents induced into the laminated or solid parts of the machine core. These additional losses depend on the operating point of the motor since they are affected by the magnitude of the armature current and the magnetic saturation of the core.

According to the standard IEEE Std 112™ from 2004 the energy loss not accounted for by the sum of friction and windage loss, the stator resistive loss, the rotor resistive loss and the no-load core loss is called the stray-load loss [1]. Up to date, no accurate models for segregating the stray-load losses to different components have been found which means that it's not actually known where the loss power is dissipated. Since the aforementioned additional losses caused by the frequency converter depend on the loading conditions and are thus a part of the stray-load losses, the contribution of the stray-load loss to the total loss of a motor is clearly higher with inverter supply than with sinusoidal supply. To reduce the losses and to improve the energy efficiency of inverter-fed electrical machines it is thus essential to understand where and why these additional losses occur and what can be done to reduce them.

The additional losses have been studied up to some extent mostly in induction and permanent-magnet synchronous machines [2]-[6]. However, inverters are becoming increasingly important also in very high-power wound-field synchronous motor drive applications. Since the total power losses in these motors can rise up to the megawatt range, it is highly important to study means of reducing the losses and enhancing the efficiency also in synchronous machine applications.

In this paper, the additional eddy-current losses in the stator and rotor cores of a large synchronous extruder motor are investigated in different loading conditions. The machine is modeled by using time-stepping 2D finite element (FE) analysis included with a model for the eddy-currents in the core laminations. The motor is simulated using both sinusoidal and pulse-width modulated (PWM) voltage supplies in different operating points and the differences in the eddy-current losses are studied.

II. Methods

A. The Lamination Model

The eddy currents in a ferromagnetic lamination oppose the penetration of the magnetic flux-density into the sheet. This phenomenon is called the skin effect, and it's described by the diffusion equation

$$\frac{\partial^2 \boldsymbol{h}(z,t)}{\partial z^2} = \sigma \frac{\partial \boldsymbol{b}(z,t)}{\partial t}, \tag{1}$$

where z is the position in the lamination depth, and the magnetic flux density $\boldsymbol{b}$ and field strength $\boldsymbol{h}$ are assumed to be parallel to the cross-sectional (xy) plane of the lamination. σ is the electrical conductivity of the lamination material.

In [7] and [8], a mesh-free lamination model was developed to describe the eddy-current effects. The model is based on approximating the flux-density distribution in the lamination depth $z \in [-d/2, d/2]$ as a

This work was supported by ABB Oy, Electrical Machines, the Walter Ahlström foundation, the Fortum foundation and the Finnish Foundation for Economic and Technical Sciences (KAUTE).

truncated Fourier cosine series with N_F terms:

$$\boldsymbol{b}(z,t)=\sum_{n=0}^{N_F-1}\boldsymbol{b}_n(t)\alpha_n(z)\,,\ \alpha_n(z)=\cos\left(2n\pi\frac{z}{d}\right). \quad (2)$$

In a similar way, the field strength is approximated as

$$\boldsymbol{h}(z,t)=\boldsymbol{h}_s(t)-\sigma d^2\sum_{n=0}^{N_F-1}\frac{\partial\boldsymbol{b}_n(t)}{\partial t}\beta_n(z) \quad (3)$$

where $\boldsymbol{h}_s(t)$ is the field strength on the lamination surface and functions $\beta_n(z)$ are defined so that $\beta_n(\pm d/2)=0$ and

$$\alpha_n(z)=-d^2\frac{\partial^2\beta_n(z)}{\partial z^2}. \quad (4)$$

With these approximations, $\boldsymbol{b}(z,t)$ and $\boldsymbol{h}(z,t)$ satisfy (1) and the surface field strength is obtained from the system

$$\begin{bmatrix}\boldsymbol{h}_s(t)\\0\\\vdots\end{bmatrix}=\frac{1}{d}\int_{-d/2}^{d/2}\boldsymbol{h}(z,t)\begin{bmatrix}\alpha_0(z)\\\alpha_1(z)\\\vdots\end{bmatrix}dz+\sigma d^2\boldsymbol{C}\frac{\partial}{\partial t}\begin{bmatrix}\boldsymbol{b}_0(t)\\\boldsymbol{b}_1(t)\\\vdots\end{bmatrix}, \quad (5)$$

in which the elements of the constant matrix $\boldsymbol{C}$ are obtained by integration over the lamination thickness as

$$C_{ij}=\frac{1}{d}\int_{-d/2}^{d/2}\alpha_{i-1}(z)\beta_{j-1}(z)\,dz\,, \quad (6)$$

The eddy-current loss density in the lamination can be calculated from the time-varying flux-density distribution as

$$\begin{aligned}p(z,t)&=\sigma\left(\int_0^z\frac{\partial\boldsymbol{b}(z,t)}{\partial t}dz\right)\cdot\left(\int_0^z\frac{\partial\boldsymbol{b}(z,t)}{\partial t}dz\right)\\&=\sigma\sum_{m=0}^{N_F-1}\sum_{n=0}^{N_F-1}(\boldsymbol{b}_m\cdot\boldsymbol{b}_n)\int\alpha_m(z)dz\int\alpha_n(z)dz.\end{aligned} \quad (7)$$

Generally the relationship between $\boldsymbol{b}(z,t)$ and $\boldsymbol{h}(z,t)$ is nonlinear and hysteretic. In addition, the excess losses could be considered locally in the lamination through this relationship. In this paper, the hysteresis and excess losses are not considered, and nonlinear but single-valued material characteristics are assumed. Only when verifying the model by comparison to measurements, a hysteresis model has to be considered.

B. Verification of the Lamination Model

The presented lamination model was verified by comparing simulated results to dynamic B-H loop measurements performed for a 0.5 mm Fe-Si lamination with a conductivity of 2.2 MS/m. A static inverted vector Preisach model [9] was used to obtain the field strength $\boldsymbol{h}(z,t)$ from the flux density $\boldsymbol{b}(z,t)$. The parameters of the hysteresis model were obtained by curve fitting to measurements with an alternating average flux-density supply. The results of the fitting are shown in Fig. 1. In Fig. 2, the loci of the measured and simulated surface field strengths are compared with a rotational 500 Hz average flux-density supply. The simulation results compare reasonably well with the measurements.

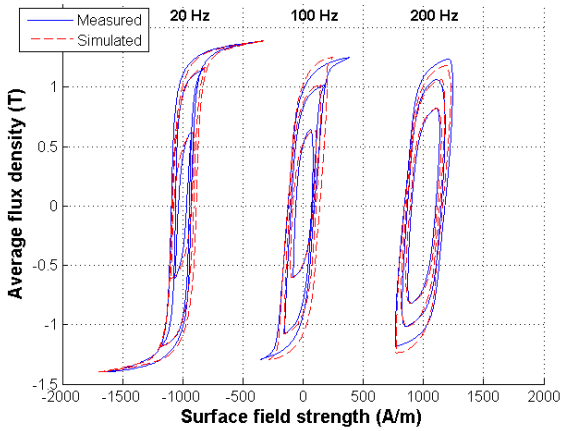

Fig. 1. Fitting the model to measured B-H curves with alternating average flux density

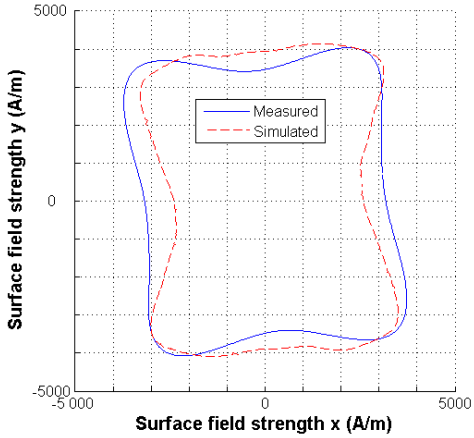

Fig. 2. 2D loci of the surface field strength with rotational 500 Hz average flux density

C. The 2D Model

In 2D finite element formulations, the Ampere's circuital law $\nabla\times\boldsymbol{H}=0$ is solved in the core regions with no source-current terms. If the magnetic field $\boldsymbol{H}=\boldsymbol{H}(x,y,z,t)$ is replaced with the surface term $\boldsymbol{H}_s=\boldsymbol{H}_s(x,y,z,t)$ obtained from the lamination model, the following system of equations is obtained:

$$\frac{1}{d}\nabla\times\int_{-d/2}^{d/2}\boldsymbol{H}\begin{bmatrix}\alpha_0\\\alpha_1\\\vdots\end{bmatrix}dz+\sigma d^2\boldsymbol{C}\frac{\partial}{\partial t}\nabla\times\begin{bmatrix}\boldsymbol{B}_0\\\boldsymbol{B}_1\\\vdots\end{bmatrix}=\begin{bmatrix}0\\0\\\vdots\end{bmatrix}. \quad (8)$$

This system can be solved in terms of the axial magnetic vector-potential components $\boldsymbol{A}_n=A_n\boldsymbol{u}_z$ corresponding to the magnetic flux-density terms $\boldsymbol{B}_n=\nabla\times\boldsymbol{A}_n$.

Discretizing the cross-section into elements with N nodes in total and applying the Galerkin weighted residual method results into a system of N_FN equations for the nodal values of the vector potential components $\mathbf{a}_n=(\mathbf{a}_{n,1},\ldots,\mathbf{a}_{n,N})$, with $n=0,\ldots,N_F-1$. The time derivatives can be handled with a suitable time-discretization method, e.g. the Crank-Nicolson approximation. Due to

the assumption of single-valued material properties, the Newton-Raphson method can be applied to solve the resulting nonlinear system effectively.

III. Application

A. The Motor Construction

The presented model was applied to calculate eddy-current losses in a 12.5 MW, 3150 V, 6-pole synchronous motor designed for an extruder application. Fig. 3 shows the 2D geometry and rated-load flux-density distribution of the motor. Rated data and some dimensions of the machine are listed in Table I.

In the simulations, the stator core laminations were assumed to have a thickness of 0.65 mm and conductivity of 2.5 MS/m. In this power class, sheets thicker than 0.5 mm are rarely used but here a 0.65 mm sheet was chosen to consider the additional losses in the worst possible case. The rotor pole lamination was of 2 mm and 8 MS/m. Thicker steel sheets with no silicon contents are often used as the rotor-pole material of synchronous machines to reduce the production costs. For long, this has been found reasonable since the magnetic field variations are negligible in most parts of the rotor. However, the air-gap flux density harmonics induce high-frequency eddy currents on the pole surface. The currents and thus also the power losses caused by them are more significant with thick and highly-conducting laminations than would be in the case if the poles were also made from the stator material. Since the use of frequency converters is continuously increasing, the traditional choice for rotor pole material could perhaps be reconsidered.

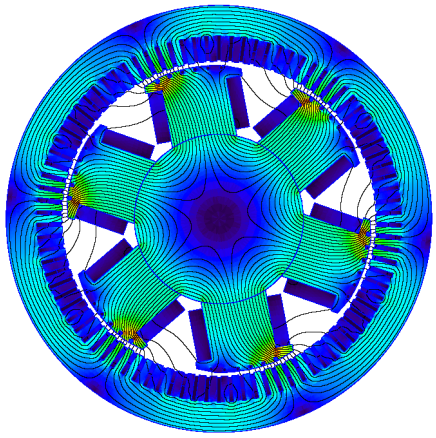

Fig. 3. Synchronous extruder motor under investigation

TABLE I
RATED DATA AND DIMENSIONS OF THE MOTOR

Shaft power	12500 kW
Voltage	3150 V
Current	2x1167 A
Power factor	1
Frequency	50 Hz
Connection	star
Number of pole pairs	3
Stator outer diameter	1820 mm
Stator inner diameter	1340 mm
Air gap	15 mm
Number of stator slots	90

B. Studied Operating Points

The motor was simulated both with sinusoidal and PWM voltage supplies. The line-to-line voltages in the PWM supply were obtained by a simple sinus-triangular comparison with a switching frequency of 300 Hz which is a typical rate for MW-range converters. Fig. 4 shows the sinusoidal supply voltages and one of the inverter-supplied line-to-line voltages.

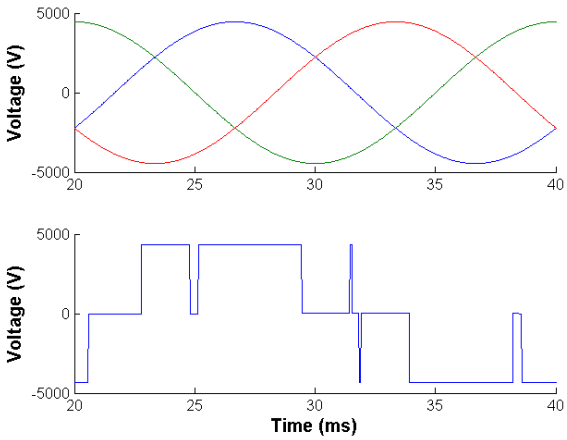

Fig. 4. Sinusoidal and PWM supply voltages

To study the effect of the loading conditions on the additional inverter losses, the machine was simulated with different shaft powers from no load up to 20 % overload operation. Both unity and 0.8 leading displacement factors were considered. The displacement factor considers the phase shift between the fundamental components of the voltage and current and describes the operating point better with the PWM supply, when the actual power factor is decreased due to the reactive power dissipation caused by the harmonic contents. In the FE simulations, 800 time steps were used per one supply period. An initial state for the time stepping was calculated by combining a static FE field solution with the two-axis motor model, and the machine was simulated for two periods to reach steady-state operation.

The skin effect was modeled with N_F = 9 cosine terms. The eddy-current losses were calculated at each time step by (7) and averaged over one supply period. The additional losses were obtained as the difference between the losses with PWM and sinusoidal supplies.

IV. Results

The machine currents in the rated-load operation both with the sinusoidal and the PWM supply are plotted in Fig. 5. With PWM supply, the currents are highly distorted which implies a high increase also in the eddy-current losses.

Fig. 6 shows the difference in the flux-density distributions of the machine with PWM and sinusoidal supplies. This difference can be considered as the high-frequency flux density caused by the inverter. The high-frequency flux does not penetrate deep into the rotor due to the damping bars which force the harmonics on the pole surface. Thus also the highest additional losses on the rotor side will occur very close to the pole surface.

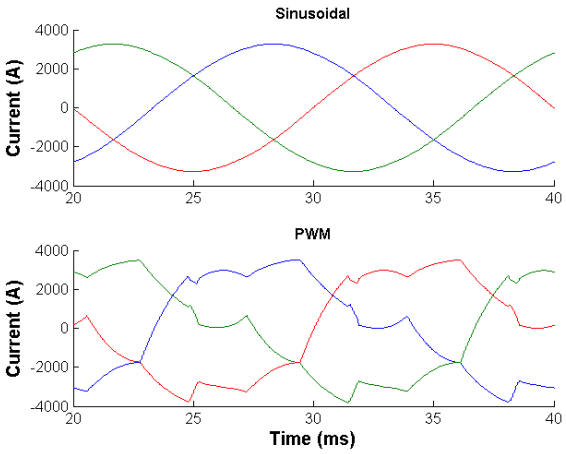

Fig. 5. Rated-load stator phase currents with sinusoidal and PWM supplies

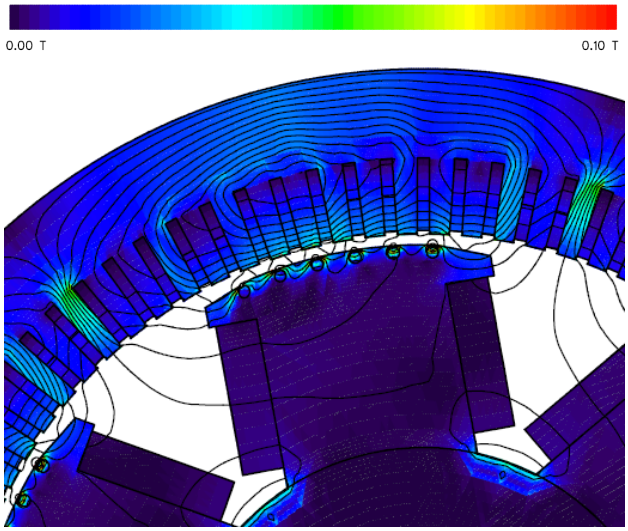

Fig. 6. High-frequency flux-density distribution in the machine

In Fig. 7, the eddy-current losses both in the stator and the rotor are plotted as a function of time. The PWM supply has a significant effect on the instantaneous eddy-current losses, even more notably in the rotor side. The difference between the PWM and sinusoidal losses is the additional inverter loss.

The dependence of the eddy-current losses on the output power of the motor is shown in Fig. 8 at unity displacement factor. The losses are averaged over one fundamental period of the supply voltage. With both sinusoidal and PWM supplies the stator losses seem to increase almost linearly with the output power while the rotor losses grow faster with higher loads.

In Fig. 9, the additional losses are plotted as a function of the motor power both at unity and 0.8 leading displacement factors. It can be noted that the additional loss in the stator remains nearly constant independent of the load. However, the rotor additional loss seems to increase by almost 40 % as the loading increases from no load to 20 % overload. The stator additional loss is also relatively small when compared to the rotor additional loss in spite of the assumption of 0.65 mm stator lamination. The displacement factor has little effect on the loss increase.

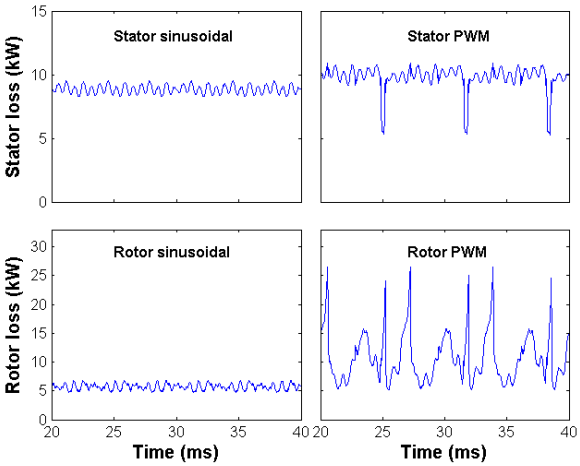

Fig. 7. Eddy-current losses in the stator and rotor on rated-load operation

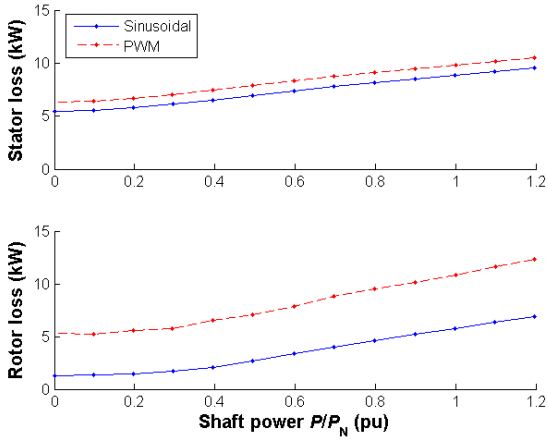

Fig. 8. Dependency of the eddy-current losses on the motor power at unity displacement factor

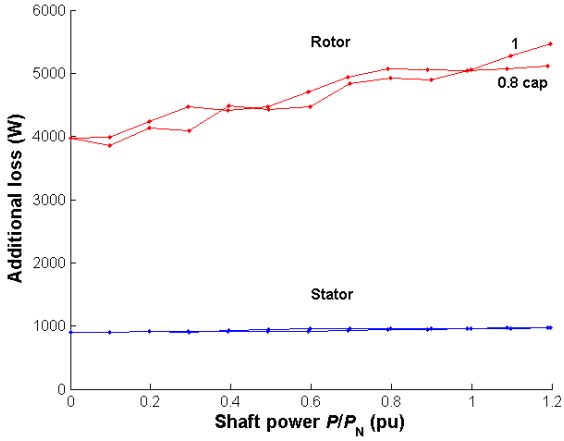

Fig. 9. Dependency of the additional eddy-current losses on the motor power at displacement factors 1 and 0.8 cap

To explain the reasons for the load-dependency of the additional inverter loss on the rotor side, the flux-density and additional-loss distributions in the rotor have to be considered. Figs. 10 and 11 present both the instantaneous flux-density and averaged additional eddy-current loss distributions in the core of the motor at no load and at rated-load operation. The coloring and the flux lines in Fig. 10 refer to the spatial average flux density $\boldsymbol{b}_0(t)$ over the lamination thickness.

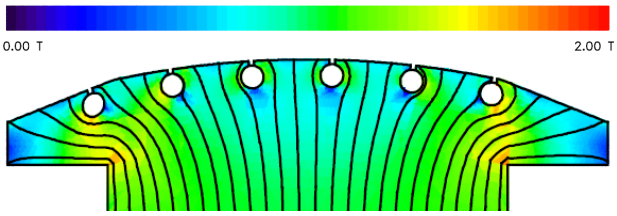

b) No-load operation

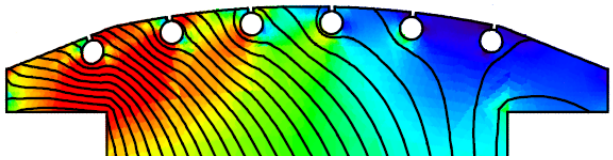

b) Rated-load operation

Fig. 10. Flux-density distributions in the pole at no-load and rated-load operation with PWM supply

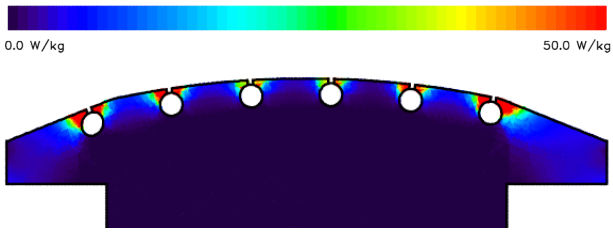

a) No-load operation

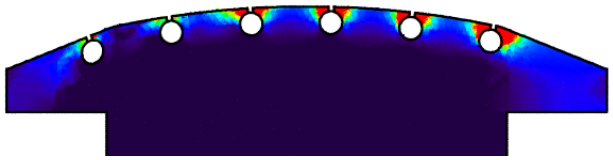

b) Rated-load operation

Fig. 11. Distributions of the additional eddy-current loss density in the rotor pole at no-load and rated-load operation

As seen in Fig. 11, the additional losses occur mostly on the pole surface above the damping bars, which force the high-frequency flux-density harmonics into the iron bridges. A bit surprisingly, it can be noted that the maximum additional inverter loss actually occurs not on the parts with the highest values of $\boldsymbol{b}_0(t)$ but on the parts with the lowest ones. This can be explained by the fact that the average flux density $\boldsymbol{b}_0(t)$ has an offset component caused by the direct current in the field winding. All the high-frequency harmonics in $\boldsymbol{b}_0(t)$ caused by the inverter are imposed over this offset component. As the offset increases, the material starts to saturate and the average reluctivity over the lamination thickness increases. This in turn reduces the significance of the skin effect in the lamination and thus the actual flux density has a more uniform distribution over the lamination thickness which reduces the eddy-current losses.

When the loading increases, the armature reaction causes the offset component to increase on the leading edge of the pole shoe and to decrease in the center and on the other edge as seen in Fig. 10. Due to this decrease in the reluctivity, the skin effect becomes more significant next to the damper bars near the center and on the right edge of the pole shoe in Fig. 11 which increases the eddy-current losses on these areas. This increase in the losses is higher than the corresponding decrease on the leading pole edge which causes the additional loss to increase when the loading increases.

V. Conclusion

The effect of inverter supply on the eddy-current losses in a laminated-core synchronous motor was studied in different loading conditions. The eddy currents in the core laminations were modeled by approximating the flux-density distribution in the lamination depth as a cosine series thus taking into account the skin effect which is significant especially in 2 mm thick rotor pole sheets. The effect of the inverter on the eddy-current losses was studied by comparing results obtained with sinusoidal and PWM supplies.

The additional eddy-current loss caused by the inverter supply is more significant in the rotor than in the stator. In addition, the rotor additional loss was found to increase with the loading of the machine, while the stator additional loss remains constant independent of the loading. The highest additional losses occur on the rotor pole surface above the damping bars on those areas, where the offset component caused by the field current has it's lowest value.

The presented findings are important to know when attempts are made to minimize the losses and to improve the energy efficiency of the machines e.g. by more accurate damper-bar or rotor pole-shape design. In addition to the classical eddy-current losses, also hysteresis and excess losses should be considered and the results should be verified by measurements.

References

[1] IEEE Power Engineering Society, "IEEE Standard Test Procedure for Polyphase Induction Motors and Generators," *IEEE Std 112™*, 2004.

[2] O. Bottauscio, M. Chiampi, A. Manzin, M. Zucca, "Additional Losses in Induction Machines Under Synchronous No-Load Conditions," *IEEE Trans. Magn.*, Vol. 40 No. 5, September 2004, pp. 3254-3261.

[3] O. Bottauscio, A. Canova, M. Chiampi, M. Repetto, "Rotational hysteresis and eddy current losses in electrical motor stators under non-conventional supply," *J. Magn. Magn. Mater.*, Vol. 254-255, January 2003, pp. 241-243.

[4] C. Cester, "Iron Loss Under Practical Working Conditions of a PWM Powered Induction Motor," *IEEE Trans. Magn.*, Vol. 33, No. 5, September 1997, pp. 3766-3768.

[5] A. J. Moses, N. Tutkun, "Localised losses in stator laminations of an induction motor under PWM excitation," *J. Mater. Process. Technol.*, Vol. 161, No. 1-2, April 2005, pp. 79-82.

[6] K. Yamazaki, Y. Seto, "Iron Loss Analysis of Interior Permanent-Magnet Synchronous Motors – Variation of Main Loss Factors Due to Driving Condition," *IEEE Trans. Magn.*, Vol. 42, No. 4, July/August 2006, pp. 1045-1051.

[7] J. Gyselinck, R. V. Sabariego, P. Dular, "A Nonlinear Time-Domain Homogenization Technique for Laminated Iron Cores in Three-Dimensional Finite-Element Models," *IEEE Trans. Magn.*, vol. 42, no. 4, April 2006, pp. 763-766.

[8] P. Rasilo, A. Arkkio, "A Mesh-Free Model of Eddy-Current Losses for 2D Analysis of Ferromagnetic Laminations," Compumag 2009, Florianopolis, Brazil.

[9] E. Dlala, J. Saitz, A. Arkkio, "Inverted and Forward Preisach Models for Numerical Analysis of Electromagnetic Field Problems," *IEEE Trans. Magn.*, Vol. 42, No. 8, August 2006, pp. 1963-1973.